

Accepted Manuscript

Copper complexes containing thiosemicarbazones derived from 6-nitropiperonal: Antimicrobial and biophysical properties



Floyd A. Beckford, Kelsey R. Webb

PII: S1386-1425(17)30327-X

DOI: doi: [10.1016/j.saa.2017.04.057](https://doi.org/10.1016/j.saa.2017.04.057)

Reference: SAA 15110

To appear in: *Spectrochimica Acta Part A: Molecular and Biomolecular Spectroscopy*

Received date: 6 November 2016

Revised date: 20 March 2017

Accepted date: 18 April 2017

Please cite this article as: Floyd A. Beckford, Kelsey R. Webb , Copper complexes containing thiosemicarbazones derived from 6-nitropiperonal: Antimicrobial and biophysical properties. The address for the corresponding author was captured as affiliation for all authors. Please check if appropriate. Saa(2017), doi: [10.1016/j.saa.2017.04.057](https://doi.org/10.1016/j.saa.2017.04.057)

This is a PDF file of an unedited manuscript that has been accepted for publication. As a service to our customers we are providing this early version of the manuscript. The manuscript will undergo copyediting, typesetting, and review of the resulting proof before it is published in its final form. Please note that during the production process errors may be discovered which could affect the content, and all legal disclaimers that apply to the journal pertain.

**Copper complexes containing thiosemicarbazones derived from 6-nitropiperonal:
antimicrobial and biophysical properties**

Floyd A. Beckford* and Kelsey R. Webb

Department of Natural Sciences, The University of Virginia's College at Wise, 1 College
Avenue, Wise, VA 24293

* Corresponding author: fab5b@uvawise.edu, Ph: (276) 376-4657, Fax: (276) 376-4603

Abstract

A series of four thiosemicarbazones from 6-nitropiperonal along with the corresponding copper complexes were synthesized. The biophysical characteristics of the complexes were investigated by the binding to DNA and human serum albumin. The binding to DNA is moderate; the binding constants run from $(0.49 - 7.50) \times 10^4 \text{ M}^{-1}$. In relation to HSA, the complexes interact strongly with binding constants on the order of 10^5 M^{-1} . The complexes also display antioxidant behavior as determined by the ability to scavenge diphenylpicrylhydrazyl (dpph) and nitric oxide radicals. The antimicrobial profiles of the compounds, tested against a panel of microbes including five of the ESKAPE pathogens (*Staphylococcus aureus*, *MRSA*, *Escherichia coli*, *Klebsiella pneumoniae*, *MDR*, *Acinetobacter baumannii*, *Pseudomonas aeruginosa*) and two yeasts (*Candida albicans* and *Cryptococcus neoformans var. grubii*), are also described. The compounds contain a core moiety that is similar to oxolinic acid, a quinolone antibiotic that targets DNA gyrase and topoisomerase (IV). The binding interaction between the complexes and these important antibacterial targets were studied by computational methods, chiefly docking studies. The calculated dissociation constants for the interaction with DNA gyrase B (from *Staphylococcus aureus*) range from 4.32 to 24.65 μM ; the binding was much stronger to topoisomerase IV, with dissociation constants ranging from 0.37 to 1.27 μM .

Keywords: Thiosemicarbazone; Antioxidant; Antibacterial; Molecular docking

1. Introduction

The development of organometallic and inorganic complexes for medicinal use is a field of emerging significance due to the diversity of coordination chemistry that is available. Frequently used for cancer treatment, cisplatin and its many derivatives have demonstrated the successful capabilities of organometallics; however, there is a crucial need for the development of alternatives to these drugs because of their harmful side effects, such as nephrotoxicity and platinum resistance [1]. Copper, which is a trace metal responsible for many important biological functions in the body, has been recognized for its many biological activities, such as antioxidant, antibacterial, antimicrobial, and antitumor behaviors, thus making it a promising candidate for anticancer as well as for other medicinal uses.

The combination of certain transition metals and ligands has been shown to have synergistic effects by either enhancing and/or resulting in new biological activities in the complexes. Thiosemicarbazone (TSC) ligands have attracted the attention of many researchers due to their antitumor, antibacterial, and antiviral properties [2-5]. Recently, the idea of incorporating biological components into the ligands themselves has led to the development of new and encouraging anticancer complexes [6]. The biologically active compound 6-nitropiperonal (NP) is known to possess antitumor and antibacterial properties, making it a structure of considerable interest for continued study. This research presents four novel ligands constituted of 6-nitropiperonal and various thiosemicarbazide units that were incorporated into the synthesis of four novel copper(II) 6-nitropiperonal thiosemicarbazone (Cu NP-TSC) complexes.

There is a variety of cellular targets that are vital to consider when investigating the biological mechanisms for metal complexes. This is in order to improve the efficacy as well as selectivity of the complexes. Human serum albumin (HSA), the most abundant protein in human blood plasma, is a carrier protein of particular interest for drug delivery because it is nontoxic and binds to a variety of compounds [7]. Since HSA plays a vital role in the transportation of drugs, it is important to understand the interactions present between the drug and protein. In this research, we have investigated the ability of the Cu NP-TSC complexes to bind to this protein. In addition to HSA, deoxyribonucleic acid (DNA) is another potentially significant biological target. For the development of less toxic yet successful metal complexes for medicinal use, it is also vital to understand the interactions and mechanisms between the metal complex and DNA. Although some copper complexes have been reported in literature to induce apoptosis [8], there is not much information currently known about the general interactions of

copper complexes with DNA. This paper investigates experimentally the interactions that the novel Cu NP-TSC complexes exhibit with DNA.

In addition, other biological targets of interest were theoretically explored. Two specific enzymes, DNA gyrase B and Topoisomerase IV, were utilized in computational studies with the complexes. These two enzymes play important roles in DNA replication and cellular growth [9]. Therefore, the ability to inhibit these enzymes is of great interest for many antibacterial studies. Computational studies were carried out for the four complexes by docking to these enzymes in order to assess their potential for medicinal use.

2. Experimental

2.1 Material and Methods

Analytical or reagent grade chemicals were used throughout. All the chemicals including solvents were obtained from Sigma-Aldrich or other commercial vendors and used as received. Microanalyses (C, H, N) were performed by Galbraith Laboratories, (Knoxville, TN). Infrared spectra in the range $4000 - 500 \text{ cm}^{-1}$ were obtained using the UATR accessory or in KBr discs on a Perkin Elmer Spectrum 100 FTIR spectrophotometer. Absorption spectra were recorded on a Perkin Elmer Lambda 25 spectrophotometer. Mass spectrometric measurements were carried out with an Advion expression-L CMS. Conductivity measurements were made on a Accumet AB200 conductivity meter. Cyclic voltammetric (CV) data were collected on a Bioanalytical Systems Inc. Epsilon potentiostat on a C3 cell stand at 296 K. DMSO solutions ($1 \times 10^{-3} \text{ M}$) containing 0.1 M tetrabutylammonium hexafluorophosphate as the supporting electrolyte. The measurements were carried out with a three-electrode system consisting of a platinum working electrode, a platinum wire auxiliary electrode and a Ag/AgCl reference electrode. The thermal analysis measurements were made on a Perkin Elmer TGA4000 instrument.

2.2 Syntheses

The ligands were synthesized according to a standard method [10,11]. Briefly, equimolar amounts of the aldehyde and the appropriate alkyl-substituted thiosemicarbazide were suspended in ethanol containing a few drops of glacial acetic acid, and the pale yellow suspension heated at reflux for 4h. After cooling to ambient temperature, the resulting bright yellow suspension was filtered and the solid washed with ethanol and air-dried. In all cases, near quantitative yields were obtained.

npTSC: Yellow solid. ESI-MS (CH_3CN) m/z $[\text{M}+\text{H}]^+$ [Observed (Calcd.)]: 268.2 (268.3). ^1H NMR (400 MHz, $\text{DMSO}-d_6$): δ 6.26 (s, 1H, H_e), 7.60 (s, 1H, H_d), 8.04 (s, 1H, H_f), 8.25, 8.32 (s, 2H, H_a),

8.47 (s, 1H, H_c), 11.65 (s, 1H, H_b); ¹³C NMR (100 MHz, DMSO-*d*₆): δ 178.3 (C₁), 151.9 (C₅), 148.6 (C₇), 143.2 (C₂), 137.4 (C₉), 125.7 (C₃), 105.9 (C₈), 104.8 (C₄), 103.6 (C₆). IR (cm⁻¹): 3417, 3229, 3152, 3100, 2948, 2795, 1601, 1538, 1517, 1474, 1383, 1322, 1266, 1100, 1036, 928, 885, 835, 825.

MnpTSC: Yellow solid. ESI-MS (CH₃CN) *m/z* [M+H]⁺ [Observed (Calcd.)]: 283.0 (283.3). ¹H NMR (400 MHz, DMSO-*d*₆): δ 6.27 (s, 1H, H_e), 7.61 (s, 1H, H_d), 8.01 (s, 1H, H_f), 8.47 (s, 1H, H_c), 8.69 (s, 1H, H_a), 11.72 (s, 1H, H_b); ¹³C NMR (100 MHz, DMSO-*d*₆): δ 177.8 (C₁), 151.8 (C₅), 148.5 (C₇), 143.1 (C₂), 136.8 (C₉), 125.8 (C₃), 105.6 (C₈), 104.8 (C₄), 103.7 (C₆), 30.9 (-CH₃). IR (cm⁻¹): 3414, 3375, 3120, 2945, 2897, 2776, 1611, 1567, 1538, 1522, 1480, 1324, 1264, 1103, 1038, 929, 887, 818.

EnpTSC: Yellow solid. ESI-MS (CH₃CN) *m/z* [M+H]⁺ [Observed (Calcd.)]: 297.0 (297.3). ¹H NMR (400 MHz, DMSO-*d*₆): δ 6.27 (s, 1H, H_e), 7.61 (s, 1H, H_d), 8.01 (s, 1H, H_f), 8.47 (s, 1H, H_c), 8.69 (s, 1H, H_a), 11.72 (s, 1H, H_b); ¹³C NMR (100 MHz, DMSO-*d*₆): δ 176.8 (C₁), 151.8 (C₅), 148.5 (C₇), 143.2 (C₂), 136.9 (C₉), 125.7 (C₃), 105.8 (C₈), 104.8 (C₄), 103.7 (C₆), 38.3 (-CH₂), 14.5 (-CH₃). IR (cm⁻¹): 3376, 3345, 3129, 2916, 1614, 1538, 1500, 1480, 1324, 1268, 1221, 1101, 1034, 928, 892, 882, 819, 801.

PnpTSC: Bright yellow solid. ESI-MS (CH₃CN) *m/z* [M+H]⁺ [Observed (Calcd.)]: 345.1 (345.4). ¹H NMR (400 MHz, DMSO-*d*₆): δ 6.28 (s, 1H, H_e), 7.65 (s, 1H, H_d), 8.21 (s, 1H, H_f), 8.60 (s, 1H, H_c), 10.25 (s, 1H, H_a), 12.05 (s, 1H, H_b), 7.53 (d, 2H, phenyl ring), 7.46 (m, 2H, phenyl ring), 7.24 (m, 1H, phenyl ring); ¹³C NMR (100 MHz, DMSO-*d*₆): δ 176.4 (C₁), 151.8 (C₅), 148.7 (C₇), 143.4 (C₂), 138.9 (C₉), 125.4 (C₃), 106.2 (C₈), 104.9 (C₄), 103.7 (C₆), {136.0, 128.1, 126.4, 125.6} (phenyl ring). IR (cm⁻¹): 3412, 3286, 2926, 1614, 1596, 1547, 1480, 1328, 1269, 1032, 924, 872, 816.

The complexes were synthesized as follows: The ligand (2 molar equivalents) was suspended in approximately 20 mL of methanol and the suspension heated to boiling. To the boiling mixture was added, dropwise, a solution of CuCl₂·2H₂O (one molar equivalent) in 5 mL methanol. The yellow mixture was heated at reflux for 2½ - 3h during which time it became a bright orange color. The reaction mixture was allowed to cool to room temperature and then filtered to collect a yellow solid. The product was washed with methanol and then a small amount of ether, followed by drying at the vacuum line.

[Cu(npTSC)₂]₂·3H₂O, **1**. Yield: yellow solid, 185 mg (73 %). Elemental analysis for C₁₈H₂₀CuN₈O₁₁S₂; Calc.: C 33.15, H 3.09, N 17.18. Found: C 33.58, H 2.37, N 16.36. ESI-MS

(CH₃CN) m/z [M + H]⁺ [Observed (Calcd)]: 599.0 (599.0). IR (cm⁻¹): 3436, 3212, 3152, 2981, 1599, 1585, 1484, 1407, 1282, 1161, 1070, 943, 883, 842, 823, 782, 730.

[Cu(MnpTSC)₂].3H₂O, **2**. Yield: yellow solid, 120 mg (50 %). Elemental analysis for C₂₀H₂₄CuN₈O₁₁S₂; Calc.: C 35.32, H 3.56, N 16.48. Found: C 35.64, H 3.03, N 15.59. ESI-MS (CH₃CN) m/z [M + H]⁺ [Observed (Calcd)]: 627.0 (627.1). IR (cm⁻¹): 3354(w), 3342, 3153, 2978, 2929, 2876, 1623, 1533, 1473, 1416, 1299, 1265, 1219, 1158, 1087, 1047, 1018, 943, 891, 840, 812, 785, 729.

[Cu(EnpTSC)₂].2H₂O, **3**. Yield: yellow solid, 150 mg (62 %). Elemental analysis for C₂₂H₂₅CuN₈O₁₀S₂; Calc.: C 38.29, H 3.80, N 16.24. Found: C 38.56, H 3.37, N 15.48. ESI-MS (CH₃CN) m/z [M + H]⁺ [Observed (Calcd)]: 655.1 (655.1). IR (cm⁻¹): 3309, 3129, 3046, 2985, 1622, 1593, 1541, 1531, 1442, 1416, 1398, 1304, 1259, 1194, 1069, 1017, 936, 889, 841, 783, 733.

[Cu(PnpTSC)₂].1½ H₂O, **4**. Yield: yellow solid, 110 mg (47 %). Elemental analysis for C₃₀H₂₅CuN₈O_{9.5}S₂; Calc.: C 46.36, H 3.24, N 14.42. Found: C 46.32, H 3.03, N 14.43. ESI-MS (CH₃CN) m/z [M + H]⁺ [Observed (Calcd)]: 751.2 (751.23). IR (cm⁻¹): 3309, 3129, 3046, 2985, 1622, 1593, 1541, 1531, 1442, 1416, 1398, 1304, 1259, 1194, 1069, 1017, 936, 889, 841, 783, 733.

2.3 Anti-oxidant assays

DPPH (2,2-diphenyl-1-picrylhydrazyl) scavenging assay: The assay was conducted in a 96-well format. The total volume of each well was 250 µL. The concentrations of the metal complex varied from 2 to 500 µM and 150 µM of dpph was added. The reactions were incubated at 25 °C for 30 minutes in the dark (shielded from light) before reading the absorbances at 520 nm. For comparisons ascorbic acid (AA) and butylated hydroxytoluene (BHT)) were incorporated onto the plates along with blanks and controls. The control was a solution of DPPH and the blank is the solvent.

Nitric oxide (NO) scavenging assay: The assay was carried out in a 96-well plate with the total well volume being 300 µL. A 100 µL aliquot of sodium nitroprusside (SNP) in phosphate buffer, was incubated with the appropriate amount of metal complex (0 – µM) for 1½ h at room temperature under light. After this period of time, 100 µL of Griess's reagent (1% sulfanilamide and 0.1% naphthylethylenediamine in 2.5% phosphoric acid) was added to each well. The

mixture was then incubated at room temperature for 10 min before the absorbance was read at 560 nm.

2.4 Antimicrobial assay

The antimicrobial activity of the complexes and ligands were assayed using three protocols.

Ligands: The ligands were tested against five bacteria and two yeasts using the following procedure carried out by the CO-ADD initiative of the University of Queensland's Institute for Molecular Bioscience. The organisms tested were bacteria *Staphylococcus aureus*, MRSA (ATCC 43300), *Escherichia coli* (ATCC 25922), *Klebsiella pneumoniae*, MDR (ATCC 700603), *Acinetobacter baumannii* (ATCC 19606), *Pseudomonas aeruginosa* (ATCC 27853); the yeasts were *Candida albicans* (ATCC 90028) and *Cryptococcus neoformans* var. *grubii*, (H99; ATCC 208821). Inhibition of bacterial growth was determined measuring absorbance at 600 nm (OD_{600}), using a Tecan M1000 Pro monochromator plate reader. For the yeasts, growth inhibition of *C. albicans* was determined measuring absorbance at 530 nm (OD_{530}), while the growth inhibition of *C. neoformans* was determined measuring the difference in absorbance between 600 and 570 nm ($OD_{600-570}$), after the addition of resazurin (0.001% final concentration) and incubation at 35 °C for additional 2 h. The absorbance was measured using a Biotek Synergy HTX plate reader. For all the microbes, the percentage of growth inhibition was calculated for each well, using the negative control (media only) and positive control (bacteria without inhibitors) on the same plate as references. The significance of the inhibition values was determined by Z-scores, calculated using the average and standard deviation of the sample wells (no controls) on the same plate. Samples with inhibition value above 80% and abs(Z-Score) above 2.5 for either replicate (n=2 on different plates) were classed as actives. Samples with inhibition value between 50-80% and abs(Z-Score) above 2.5 for either replicate (n=2 on different plates) were classed as partial actives. Negative inhibition value mean that the growth rate (or OD_{600}) is higher compared to the control (bacteria only, set to 0% inhibition).

Complexes: For the determination of inhibition zones, the disk diffusion antibacterial screenings were performed using Miller-Hinton Agar (MHA) for all the bacterial strains. The appropriate amount of the complexes was dissolved in DMSO to make of a solution that was approximately 2 mM. A suspension of the bacterial cultures with exponentially growing cells (100 - 200 μ L) was adjusted to the equivalent of a 0.5 McFarland Turbidity standard using sterile saline solution. The suspension was swabbed over the entire surface of the plated-medium using cotton swabs. Sterile paper disks (6 mm in diameter) were saturated with 30 μ L of the compounds and placed onto the plate. One disk, saturated with 30 μ L of DMSO, was placed on the plate to serve as a

negative control. A disk saturated with 15 μL of 4.67 mM ampicillin was used as a reference standard to determine the sensitivity of each strain. The inoculated plates were incubated upside-down at 37 $^{\circ}\text{C}$ for 18–24 h. The antibacterial activity was measured as the diameter (mm) of the clear zone of growth inhibition. Each plate was run each in duplicate.

The *in vitro* antimicrobial activity of the four complexes was tested against *S. aureus*, *E. coli*, *K. pneumoniae*, *P. aeruginosa*, *E. faecalis* and *B. cereus*. The bacteria were maintained on nutrient agar and cultured in Mueller Hinton Broth and compounds were dissolved in DMSO. The percent inhibition was determined from a microdilution method. Approximately 50-mL of bacteria culture was incubated overnight at 37.0 $^{\circ}\text{C}$ to produce exponentially growing cells. This was then diluted to yield a suspension containing 1.5×10^8 CFU/mL (based on comparison of the turbidity to a 0.5 McFarland standard). Subsequently, 200 μL of this bacteria mixture were then inoculated into a sterile 96-well microplate. Various amounts of the compounds were added to the wells to give predetermined concentrations ranging from 20 – 180 μM . The well absorbances (at 620 nm) were recorded on a Fisher Scientific Multiskan MCC microplate reader immediately after inoculation. The microplates were then incubated for 24 h at 37.0 $^{\circ}\text{C}$, and the absorbance read again. Solvent, negative and positive growth controls were included on each plate. Ampicillin was used as a standard comparison. Each plate contained three replicates of each concentration. The percent inhibition was calculated from the equation below.

$$\% \text{inhibition} = \left(\frac{\text{Abs}_{\text{bacteria}} - \text{Abs}_{\text{bacteria+complex}}}{\text{Abs}_{\text{bacteria}}} \right) \times 100$$

2.5 DNA-interaction studies

All the experiments involving the interaction of the complexes with DNA were carried out in TRIS buffer (5 mM Tris, 50 mM NaCl, pH 7.20). The solutions of DNA were made by dissolving the nucleic acids in the buffer. After an appropriate dilution, the concentration (per nucleotide phosphate) was determined spectrophotometrically using the molar absorption coefficient of $6600 \text{ M}^{-1} \text{ cm}^{-1}$ at 260 nm [12]. The solutions were deemed to be pure, (free of protein), since a ratio of absorbance at 260 and 280 nm was ≥ 1.8 [13]. The DNA stock solutions were stored at 4 $^{\circ}\text{C}$ and used within 4 days after their preparation. Purified water (18.2 μS) was used in all the experiments.

2.5.1 Absorbance titration experiments

Electronic absorption titrations were carried out at room temperature to investigate the binding between the complexes and ct-DNA. A constant concentration of the complexes (1.0×10^{-5} M) was treated with aliquots of a stock concentrated solution of the DNA in a 1-cm quartz cell. A sample of buffer in the reference cell was titrated in the same manner simultaneously.

2.5.2 Fluorescence titration experiments

In the ethidium bromide (EB) fluorescence displacement experiment, a buffered solution that contained $10 \mu\text{M}$ DNA pre-treated with EB ($0.66 \mu\text{M}$), was titrated with a concentrated solution of the complex. After each addition, the solution was stirred at the appropriate temperature for 5 minutes before the fluorescence measurement was taken by exciting at 520 nm and measuring the emission spectra from 530 – 700 nm.

2.6 Reaction with human serum albumin (HSA)

For the fluorescence titration, a similar procedure to the EB displacement experiments was done. Solutions of HSA (fatty acid-free) were prepared in TRIS buffer (50 mM Tris, pH 7.40, 100 mM NaCl) and stored in the dark at $4 \text{ }^\circ\text{C}$. The protein concentration was determined spectrophotometrically and calculated using the molar absorptivity of $3.6 \times 10^4 \text{ M}^{-1} \text{ cm}^{-1}$ at 280 nm [14]. In the experiments, a 3.0 mL solution of HSA ($5 \mu\text{M}$) was titrated with aliquots of a concentrated solution of the complex. The complex concentration in these mixtures ranged from 3 to $30 \mu\text{M}$. The fluorescence spectra of the solutions were obtained by exciting at 295 nm and measuring the emission spectra from 300 – 500 nm.

3. Discussion

3.1 Synthesis and characterization

The compounds used in this study have been characterized by elemental analysis as well as NMR (ligands), infrared and electronic absorption spectrophotometry. In addition, cyclic voltammetry, thermogravimetric analysis as well as conductivity measurements, were performed on the metal complexes. The ligands were synthesized by the acid-catalyzed condensation of the thiosemicarbazide with the appropriate aldehyde in refluxing ethanol and were obtained as bright yellow solids. The complexes were synthesized by refluxing the ligands with the copper salt in methanol (Fig. 1). The complexes were also obtained as yellow solids. The compounds are soluble in solvents such as DMSO and acetone but not very soluble in alcohols.

The proposed structural formulations of the ligands are consistent with their NMR spectra. All the ligands have a number of common features and they are reflected in the proton and carbon spectra. The benzodioxole moiety is of course present in all the ligands and the signals arising from this moiety is indeed common to all. For the most part, *npTSC*, *MnpTSC* and *EnpTSC* show very similar chemical shifts while *PnpTSC* show a little variation. In the proton NMR, the $-\text{CH}_2$ group (H_e) show at 6.26 ppm in all the ligands. The azomethine proton (H_b), is present at

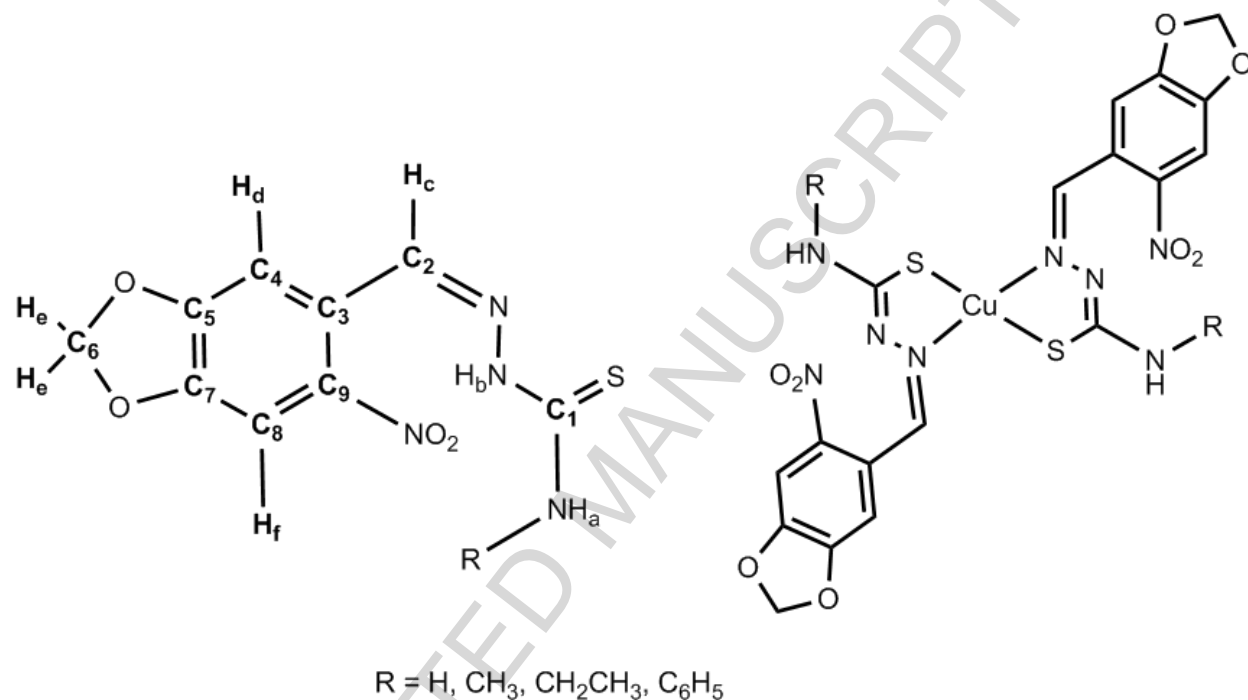


Fig. 1. Structure of the ligands and complexes synthesized in the study.

approximately 11.70 ppm for *npTSC*, *MnpTSC* and *EnpTSC* while occurring at 12.05 ppm for the *PnpTSC* compound. The presence of this peak confirms that the ligands are in the thiol tautomeric

form in solution. The aldehydic proton (H_c) resonate at 8.47 ppm (8.60 ppm for *PnpTSC*) and the other protons on the benzene ring (H_d , H_f) are consistently at 7.61 ppm and 8.04 ppm respectively (8.20 ppm for *PnpTSC*). The amine proton (H_a) has distinct behavior. In *npTSC*, we observe a singlet for each of the two protons (at 8.25 and 8.32 ppm). This is not quite unexpected as thioamides display hindered rotation about the $(\text{S}=\text{C})-(\text{NH}_2)$ bond. This is a consequence of the bond possessing some p -character with the end-result being that the two protons are magnetically non-equivalent. For *MnpTSC* and *EnpTSC*, this proton shows at 8.69 ppm but is found at a much higher frequency (10.25 ppm) for *PnpTSC*. For the substituent

groups on the amine nitrogen, the protons show at what would be considered typical for those groups.

The ^{13}C NMR supports the proton data. In all the ligands there is a very high frequency peak near 177 ppm which is easily attributable to the thiocarbonyl ($\text{C}=\text{S}$) group. This group seems relatively insensitive to the substitution on the adjacent amine nitrogen, (unlike the protons). The signals for the other carbons in the piperonal fragment occur in typical regions. For example, the $-\text{CH}_2$ group (C_6) will have its peak near 104 ppm, the high frequency being a consequence of being sandwiched between two electronegative oxygen atoms. The carbons of the amine substituent groups are also typical.

Like an imine or a typical ketone, a thiosemicarbazone may display two tautomeric forms. Consequently, thiosemicarbazone ligands can coordinate as a neutral species or as a monoanionic species. We conclude from the characterization data that the ligands are obtained as the thiol tautomer; however, they are deprotonated when they coordinate to the metal center. The complexes are therefore neutral compounds. This was verified by conductivity measurements on 1 mM DMSO solutions of the complexes. The values determined were 13.37 $\mu\text{S}/\text{cm}$, 16.26 $\mu\text{S}/\text{cm}$, 14.30 $\mu\text{S}/\text{cm}$ and 14.15 $\mu\text{S}/\text{cm}$ for **1**, **2**, **3** and **4**, respectively. They confirm the non-electrolytic nature of the complexes [15]. (Electrospray ionization) mass spectrometry on the complexes also supports the formulation of the complexes as neutral species. Peaks were observed for the complexes as follows: **1**, m/z 599.0 (calc. 599.04), $[\text{M}+\text{H}]^+$; **2**, m/z 627.09 (calc. 627.0), $[\text{M}+\text{H}]^+$; **3**, m/z 655.1 (calc. 655.14), $[\text{M}+\text{H}]^+$; and, **4**, m/z 751.23 (calc. 751.2), $[\text{M}+\text{H}]^+$. Further evidence for the composition of the complexes comes from spectroscopic methods. The infrared spectrum of the complexes has the telltale signatures of chelation through the azomethine nitrogen and the thiol sulfur [16]. The UV-vis spectrum of the complexes indicates coordination through the sulfur as well (Fig. S1, Electronic Supplementary Information, ESI). The ligands show a band at 325 nm which we interpret to be the result of the $\pi \rightarrow \pi^*$ transition of the $-\text{C}=\text{S}$ group. This band shifts to higher energies by as much as 6 nm in the spectra of the complexes. The shoulder that appears in the spectra of the ligands near 387 nm completely disappears in that for the metal complexes. The cyclic voltammogram for the complexes (Fig. 2) show one irreversible oxidation peak. The peak, which is somewhat ill-defined for **1** and **3**, occur at potentials of 1.25 V and 1.20 V, respectively. For **2** and **4**, the peak is at 1.20 V and 1.15 V respectively. The values remained essentially constant when the scan rate was changed from 100 mV/s to 200 mV/s.

3.2 Thermal analysis measurements

The thermal behavior of the complexes was investigated by thermogravimetric analysis. Fig. 3 shows the heating profile of the complexes when heated from 40 °C – 900 °C. It appears from the figure that there are three significant events happening in this range. Of particular interest are the first two since it might be suggested that the third has not been completed before the end temperature. The differences between the complexes is a matter of when the events start and the transition temperature of the particular event. For convenience, we have divided the thermogram into two parts: 200 – 335 °C and 350 – 530 °C. The transition temperatures for the first (major) stage are 263.32 °C, 256.77 °C, 261.63 °C and 251.61 °C for **1**, **2**, **3** and **4** respectively. It is obvious from the figure that complex **1** has the sharpest transition – starting at 263.01 °C and

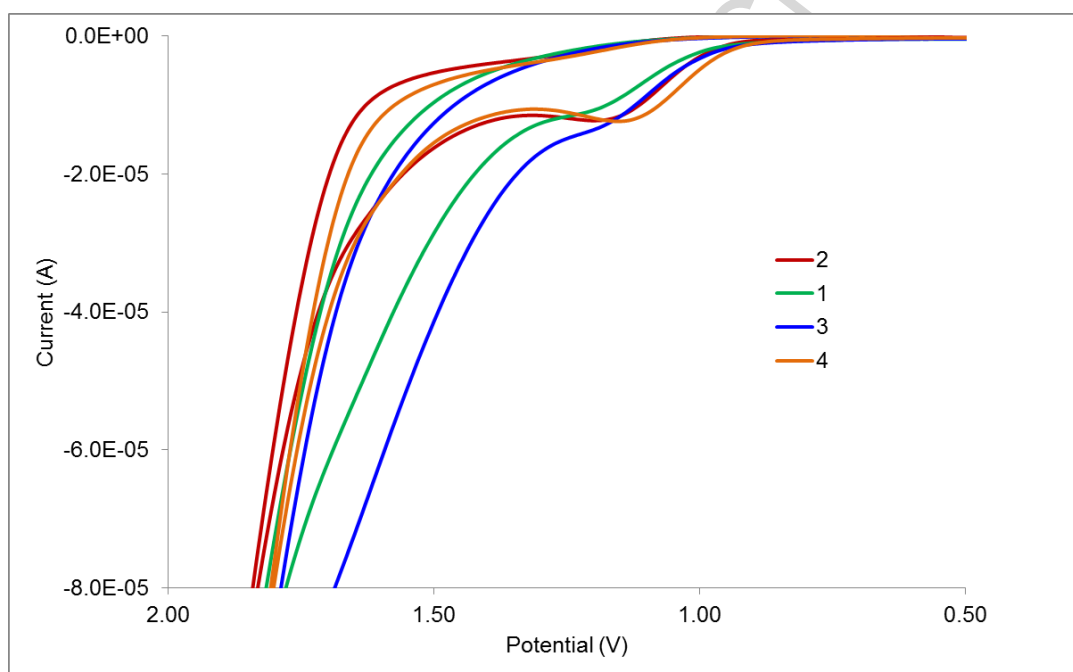


Fig. 2. Cyclic voltammograms for all four complexes measured in (1×10^{-3} M) DMSO (vs. Ag/AgCl).

ending at 264.10 °C. In this range, the material lost 36.7 weight percent. The transitions for the other complexes are not as sharp with ranges of 19 °C (20.7 weight %) for **2**, 12 °C (23.0 weight %) for **3**, and 28 °C (22.2 weight %) for **4**. We propose that the transition in this event is the result of the melting of the complexes. This is supported by the fact that the weight loss of the complexes does not correlate well with decomposition of the complexes with concurrent loss of a ligand. The second minor stage is even more unexplainable. The events are obvious but not very well defined. With our analysis methodology, the derived transition temperatures range

from 512 °C – 524 °C with one exception, 360.67 °C for **3**. The weight loss in these transitions does not exceed 9% (range: 3.7 – 8.8).

3.3 Structure description

The calculated structures of the complexes were computed by density functional theory using the ω B97X-D method and a basis set of 6-31G*. This was done using Spartan 14 [17] and in this software package, this mentioned basis set corresponds to 6-31G* on atoms smaller than krypton and LANDL2DZ on atoms larger than krypton. Fig. 4 shows the structure calculated for complex **1**. We describe this geometry as a severely distorted tetrahedron around the copper center.

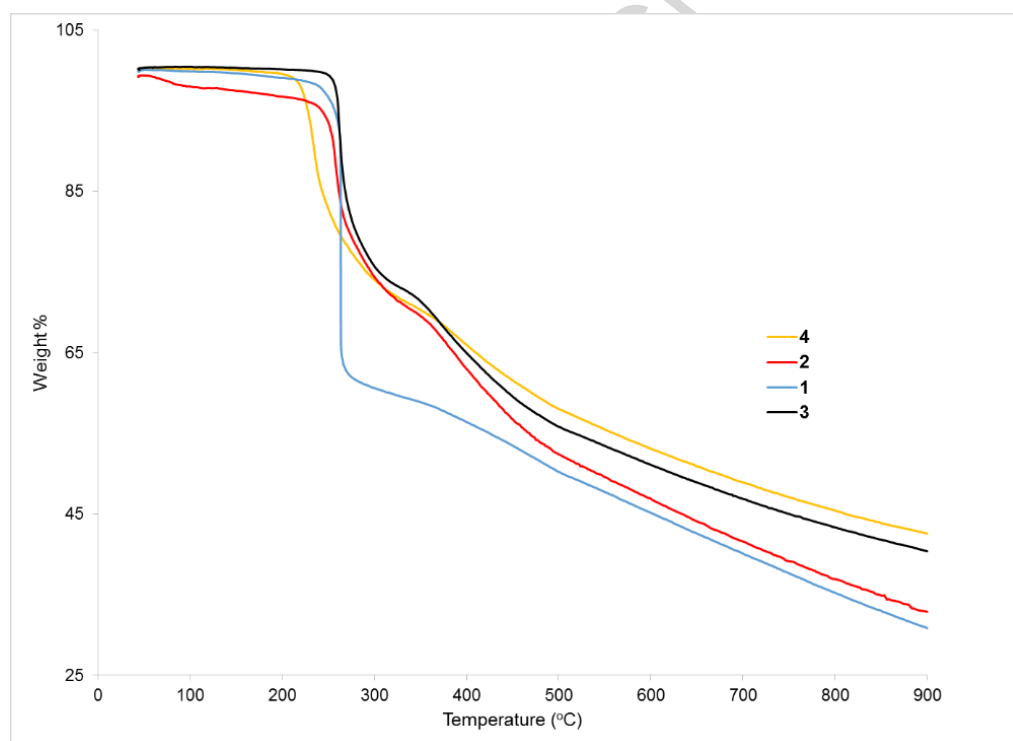


Fig. 3. TGA curves of the four complexes heated under a nitrogen atmosphere.

The coordinating fragment of the thiosemicarbazone ligands is at angle of 122.89° to each other. Some selected geometric parameters from the calculations are shown in Table 1. Amongst all four complexes, the overall shape is not significantly different, suggesting that the alkyl group on the amine nitrogen has no bearing on the geometry at the copper center. The benzodioxole moiety of the ligands is essentially flat; the oxygen of the nitro groups are twisted out of the plane by 21.86° and 32.74° in the two cases. This is seen in the free ligands as well. Relative to the coordinating fragment, this moiety is out of plane by 18.09° in one ligand and

26.39° in the other. The two ligands are close to each other and this might have an effect on the coordinating ability to macromolecules.

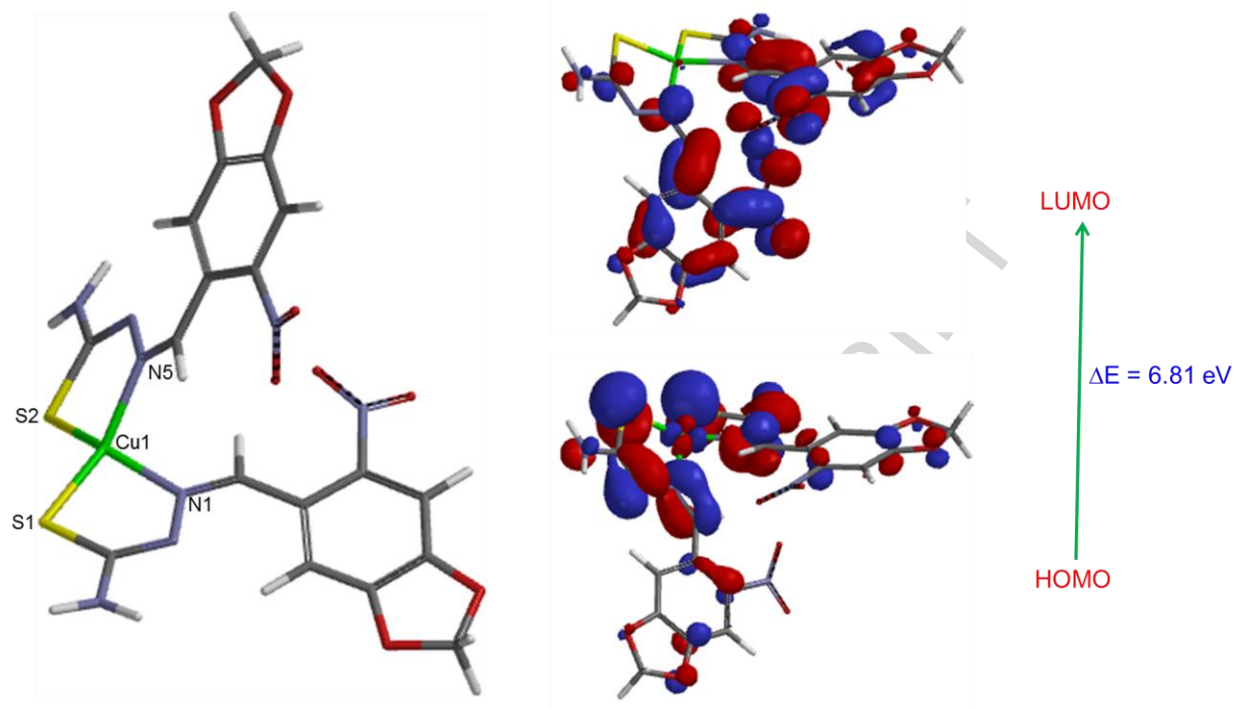


Fig. 4. Calculated structure of complex **1** along with graphical representations of the highest occupied (HO) and lowest unoccupied (LU) molecular orbitals (MO)

Table 1 Selected calculated geometrical parameters for the complexes

	1	2	3	4
Bond distances (Å)				
Cu(1)-S(1)	2.246	2.249	2.246	2.244
Cu(1)-S(2)	2.246	2.246	2.244	2.242
Cu(1)-N(1)	1.980	1.987	1.986	1.983
Cu(1)-N(5)	1.980	1.976	1.975	1.974
Bond angles (°)				
S(1)-Cu(1)-N(5)	147.15	149.65	149.52	149.43
S(2)-Cu(1)-N(1)	147.21	147.19	146.84	147.86
S(2)-Cu(1)-N(5)	86.61	86.92	86.93	86.93
S(1)-Cu(1)-N(1)	86.61	86.40	86.42	86.31
S(1)-Cu(1)-S(2)	107.51	103.18	103.34	103.25
N(1)-Cu(1)-N(5)	97.29	100.59	100.64	100.37

As might be expected, complex **5** is larger than **1** by about 1.5 times. Other (calculated) quantitative structure activity relationship parameters are essentially the same; for instance, there are zero hydrogen bonded donors and sixteen hydrogen acceptors in each complex. The frontier molecular orbitals (FMO) of a coordination complex play an important role in its reactivity. The specific HOMO and LUMO for the complexes are quite similar and Fig. 4 show those for **1**. The HOMO (-7.5415 eV) is heavily localized on the coordination sphere around the metal ion with the s and p_x orbitals on N2 and p_z orbitals on S1 the major orbitals; the six-membered ring of the benzodioxole part (including the nitro groups) of the ligand appears to bear most of the LUMO (-0.73336 eV). This is applicable to all the complexes. The negative energies of all the FMOs indicates the stability of the complexes [18]. The energy gap between HOMO and LUMO, (ΔE), suggests the chemical reactivity of compounds. The presence of the alkyl group substituted onto the amine nitrogen, appears to have some influence on the electronic characteristics of the complexes. ΔE decreases as the substituent changed from -H to $-C_6H_5$. For **1**, ΔE was 6.81 eV and that decreased to 6.39 eV in the complex bearing the methyl-substituted ligand. The differences for **2**, **3** and **4** were subtler, with $\Delta E = 6.37$ eV and 6.33 eV for **3** and **4**, respectively.

3.4 Electronic absorption titration

By using UV-Vis spectroscopy, it is possible to examine the strength of the binding interactions of metal complexes with DNA [19-21]. A cursory look at the structure of the thiosemicarbazone ligands used in the complexes would preclude the binding of the complexes to DNA via an intercalative mode. As mentioned below, small molecules can bind to DNA via an intercalation mode. This mode of binding is usually favored by the presence of a planar, extended fused aromatic (polyaromatic) ligand. To intercalate into DNA, a planar molecule slides between two base pairs without disrupting the hydrogen bonds and typically involve significant p-electron overlap. For metal complexes, binding modes to DNA may be more complicated than for simple organic molecules. For instance, intercalation may be initiated by entry to the DNA via the grooves. Consequently, it may be that for our situation neither intercalation, nor groove binding are unambiguous or independent concepts. Ordinarily, complexes which adopt this method of binding generally have electronic absorption bands that show bathochromic changes relative to the free complex and also display hypochromism

[22,23]. For our complexes, the calculated structures (Fig. 4) suggest that the thiosemicarbazone moieties are relatively planar, the methylene of the dioxole ring obviously being sp^3 and the nitro groups slightly out of the plane. So we investigated the possible binding modes for the complexes via a titration where the changes in the absorption of solutions with a fixed complex concentration (10^{-4} M), were measured upon addition of aliquots of a concentrated solution of ct-DNA. Fig. 5 shows the absorption spectra of complex **1** upon titration with ct-DNA. There is a 13% decrease in the absorption at the wavelength of maximum absorption (294 nm). A small red shift of three nanometers accompanies this decrease. The other complexes exhibit similar behavior with % hypochromicity of approximately 8% and basically no wavelength change (figures shown in the Supplementary Information). To calculate the binding strength, equation 1 [19], was used to calculate the intrinsic binding constant K_b .

$$\frac{[DNA]}{\varepsilon_a - \varepsilon_f} = \frac{[DNA]}{\varepsilon_b - \varepsilon_f} + \frac{1}{K_b(\varepsilon_b - \varepsilon_f)} \quad (1)$$

where ε_a , ε_f and ε_b corresponds to the molar absorptivities of the metal complex after each addition of ct-DNA, for the free metal complexes and for the metal complexes when completely bound. The binding constants K_b are calculated from the plots of $[DNA]/(\varepsilon_a - \varepsilon_f)$ versus $[DNA]$ taking the ratio of the slope to the intercept. These values are shown in Table 2. The binding constant are on the order of 10^4 M $^{-1}$ which, compared to a classic organic-type intercalator, characterizes them as moderate binders. The nature of the results suggests that the complexes do not interact with DNA via intercalation or at least this type of interaction is weak.

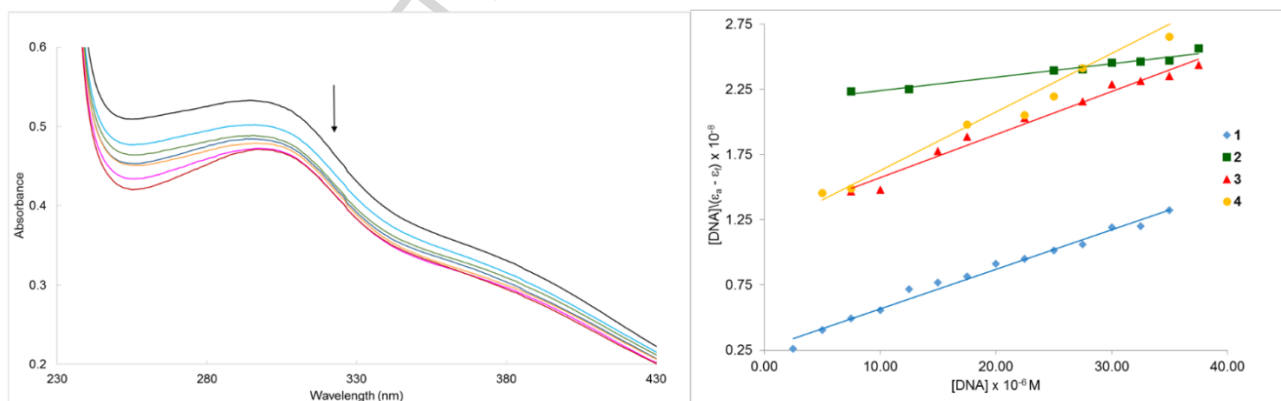


Fig. 5. Left: Electronic absorption spectral changes of complex **1** on titration with ct-DNA. $[Cu] = 25 \mu\text{M}$, $[DNA] = 0, 5, 10, 15, 20, 25$ and $30 \mu\text{M}$. Arrow indicates the change upon increasing DNA concentration. Right: Plot of $[DNA]/(\varepsilon_a - \varepsilon_f)$ vs. $[DNA]$

3.5 Ethidium bromide competition experiment

As mentioned above small molecules may interact with DNA by binding in the grooves, intercalating between the base pairs or by electrostatically interacting with the phosphate backbone if charged. One experiment commonly used to investigate a potentially intercalative

Table 2 Stern-Volmer quenching along with binding parameters for the interaction of the complexes with ct-DNA

Complex	Ethidium bromide titration			UV-vis titration
	$K_{app} \times 10^4 \text{ M}^{-1}$	$K_{SV} \times 10^4$	$K_q \times 10^{11} \text{ M}^{-1}\text{s}^{-1}$	$K_b \times 10^4 \text{ M}^{-1}$
1	1.26	2.03	9.24	7.50
2	0.825	0.753	3.42	0.485
3	1.20	1.34	6.20	2.40
4	0.881	0.842	3.82	4.26

mechanism is the ethidium bromide displacement experiment. Both DNA and ethidium bromide (EB) are non-emissive in aqueous solution; however, when they interact, the EB intercalates into the DNA molecule generating an adduct that is fluorescent. This fluorescence may be quenched if an added compound can displace the EB from the binding sites on the DNA (returning to the non-emissive states). We can see from Fig. 6 that all the complexes reduced the fluorescence of the EB-DNA solution (indicated by the arrow).

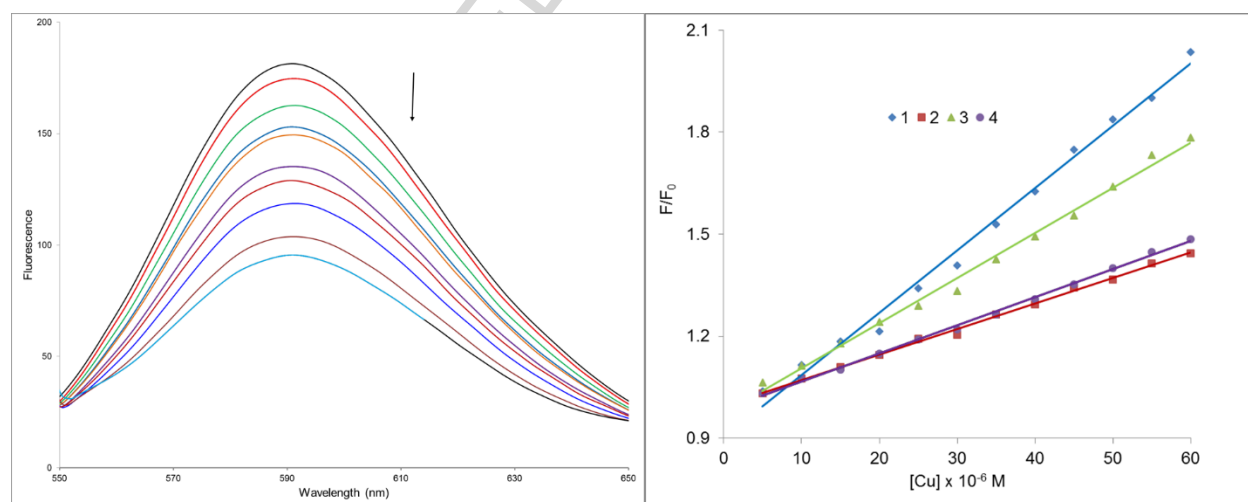


Fig. 6. Left: Fluorescence spectra of the EB-DNA complex in the absence and presence of increasing amounts **1**, $\lambda_{ex} = 520 \text{ nm}$, $[\text{EB}] = 0.33 \text{ }\mu\text{M}$, $[\text{DNA}] = 10 \text{ }\mu\text{M}$, $[\text{M}] (\text{ }\mu\text{M})$: 0 – 50 in 5 μM increments. Arrow indicates the change upon increasing complex concentration. Right: Stern-Volmer plots for all the complexes

Using the Stern-Volmer equation (equation 2), the quenching constant for the various complexes can be calculated.

$$\frac{F_0}{F} = 1 + K_{SV}[\text{Cu}] = 1 + K_q \tau_0 [\text{Cu}] \quad (2)$$

F_0 and F are the fluorescence intensities of the ethidium bromide-DNA solution in the absence and presence of the metal compound. K_{SV} is the Stern-Volmer quenching constant. The expected linearity of the plot (F_0/F vs. $[\text{Cu}]$) was observed for all three complexes with quenching constants on the order of 10^4 M^{-1} (Table 2). A linear Stern-Volmer plot is generally indicative of a single class of fluorophores, all equally accessible to quencher. This is not unexpected in our system as the complex is essentially breaking up a fluorescent adduct consisting of an intercalated EB molecule. The mechanism of this process can be collisional or through complex formation. Collisional quenching of fluorescence occurs when the quencher bumps into the fluorophore and deactivates the excited state. Static quenching occur as a result of the formation of a non-fluorescent ground-state complex between the fluorophore and quencher.

It should be noted that static quenching also results in linear Stern-Volmer plots and therefore the observation of a linear Stern-Volmer plot does not prove that the fluorescence was quenched via a collisional mechanism. Both mechanisms can be described by the Stern-Volmer equation but the K_{SV} would be best described as an association constant in the static case. [24] Intensity measurements alone cannot differentiate dynamic or static processes; the true type of quenching can be shown using lifetime measurements [24]. In our case, we can certainly speculate that static quenching is indeed a possibility by looking the bimolecular quenching constant, K_q in equation 2. Values of this parameter larger than the diffusion-controlled limit usually indicate some type of binding interaction. Table 2 also display the values of K_q which is built into the K_{SV} and reflects the degree of quenching efficiency or the accessibility of the fluorophores to the quencher. The size of the values, calculated by using $\tau_0 = 22 \text{ ns}$ [25], are about $10^{11} \text{ M}^{-1} \text{ s}^{-1}$ which is larger than the limiting value of $10^{10} \text{ M}^{-1} \text{ s}^{-1}$ [24].

To assess the strength of the binding, equation 3 was employed to calculate the apparent binding constant.

$$K_{app} = \frac{K_{EB}[\text{EB}]}{[\text{Cu}]_{50\%}} \quad (3)$$

In this equation, K_{EB} is the binding constant for ethidium bromide, taken as $1.2 \times 10^6 \text{ M}^{-1}$, [26] and $[\text{Cu}]_{50\%}$ is the concentration of the complex that causes a 50% reduction of the initial fluorescence. These values are shown in Table 2 and are on the order of 10^4 M^{-1} which suggest

that the complexes are weak to binders when one compares them to a classical intercalator. A typical intercalator like ethidium bromide has a binding constant of $3.0 \times 10^6 \text{ M}^{-1}$ [27]. This is not unexpected, as the complexes do not have the structural characteristics that are common for intercalators. The similarity in values for K_{SV} and K_{app} lend support for the idea that complex formation is a major player in the quenching of the fluorescence.

3.6 Interaction with human serum albumin

As the principal extracellular protein of the circulatory system, human serum albumin (HSA) serves as the major transporter of drugs as well as endogenous compounds. It has been shown that major pharmacokinetic parameters of drugs can be significantly altered because of their binding to HSA. Since HSA serves as a transport carrier for drugs, it is important to study the interactions of a potential drug with this protein. In this study, we investigated the binding of the complexes to HSA using fluorescence spectroscopy. HSA has a well-known structure consisting of a single polypeptide chain. The secondary structure has three homologous domains, each consisting of two subdomains. Generally speaking, the main binding sites of the protein, site I and site II, are located on subdomains IIA and IIIA. The primary structure of the protein has a single tryptophan residue at position 214 (site I) along with a number of tyrosine and phenylalanine residues. All three amino acids are emissive but tryptophan \gg tyrosine $>$ phenylalanine with respect to fluorescent intensity [24]. Consequently, most of the intrinsic fluorescence of HSA is due to the single tryptophan residue. While tyrosine residues may contribute significantly to the protein fluorescence, by appropriate choice of the exciting wavelength it is theoretically possible to isolate the tyrosine fluorescence. In addition, the wavelength of the emitted light is a good indication of the environment of the fluorophore. Tryptophan residues that are exposed to an aqueous environment, have maximal fluorescence at a wavelength of about 340-350 nm; residues in the interior of the proteins, fluoresce at about 330 nm. Therefore, the fluorescence titration is a good investigative method for binding as this emission can be attenuated by a small molecule interacting at or near the tryptophan; this amino acid unit is quite susceptible to changes in its micro-environment.

Fig. 7(a) show the fairly large reduction in fluorescence intensity associated with a solution of HSA upon addition of aliquots of complex 1. All the complexes display this behavior (ESI). This is indicative of some sort of binding interaction at or near the tryptophan residue. It was also observed that there is a small red shift of about 0 - 6 nm for the complexes. It is therefore likely that the interaction of the complexes with the protein has resulted in changes in the secondary structure of the protein. It appears that the tryptophan residue is becoming more

exposed to the polar environment. The strength of the binding may be quantified using the Stern-Volmer equation (4).

$$\frac{F_0}{F} = 1 + K_q \tau_0 [Cu] = 1 + K_D [Cu] \quad (4)$$

K_q is the bimolecular quenching constant and τ_0 is the lifetime of the fluorophore in the absence of complex. The Stern-Volmer quenching constant is given by $K_D = K_q \tau_0$ a representation of the

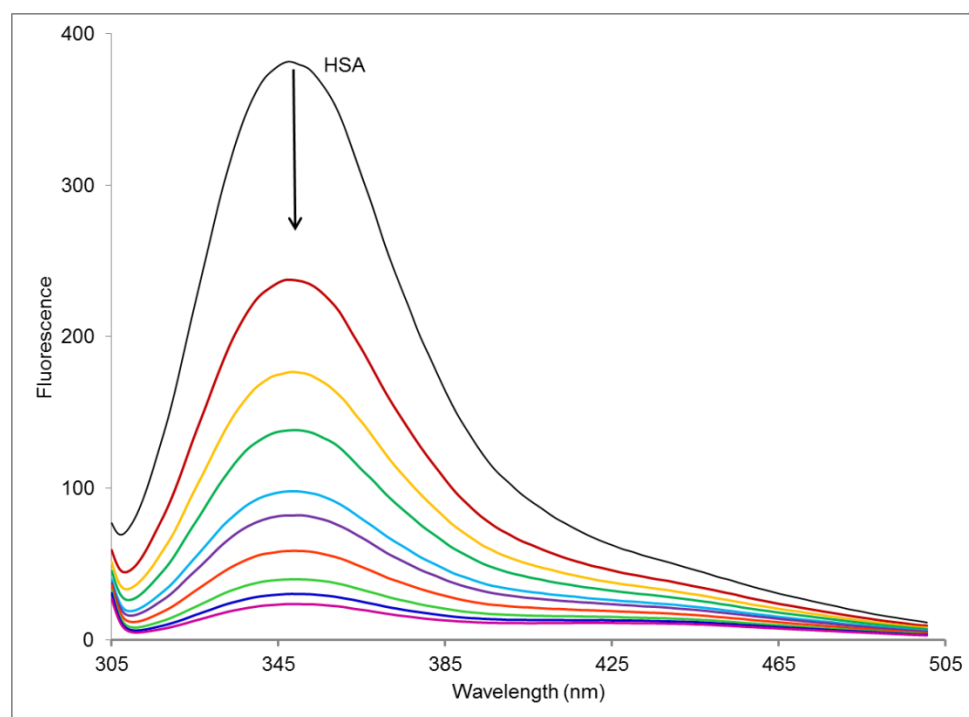


Fig. 7. Emission spectra of HSA in the absence and presence of increasing amounts of **1**, $\lambda_{ex} = 295$ nm, $[HSA] = 5.0$ μM and $[1]$ (μM): 0 – 22.5 in 2.5 μM increments.

K_{SV} if the quenching is known to be dynamic. K_{SV} is the measure of the effectiveness of the complex as a quencher.

As seen in Fig. 8, the Stern-Volmer plot shows a distinct upward curvature. For protein solutions having homogeneous emission, upward curvature has been observed with a wide variety of quenchers [24]. In fact, the fluorescence of most proteins is likely heterogeneous [29]. Since linearity of a Stern-Volmer plot is usually associated with the fluorophore possessing a single binding site or multiple accessible binding sites, we suggest that deviation from linearity is due to the occurrence of combined quenching sites and/or the existence of non-equivalent (different or same (accessible or non-accessible)) binding. Combined quenching implies that

static quenching can occur simultaneously to the dynamic quenching mechanism that governs the Stern-Volmer plot. The static contribution may be calculated from the following equation:

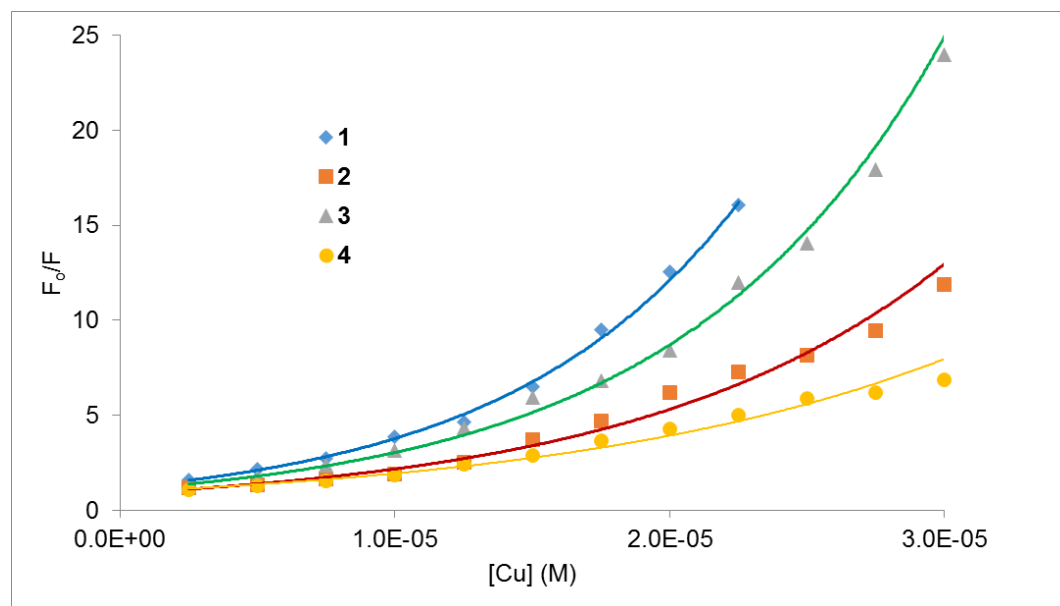


Fig. 8. Stern-Volmer plots for the interaction of the complexes HSA.

$$\frac{F_0}{F} = (1 + K_D[Cu])(1 + K_S[Cu]) \quad (5)$$

In this equation, K_D and K_S are the dynamic and static quenching constants. This is a modified form of the Stern-Volmer equation applicable when one is considering the same population of fluorophores [24].

$$\frac{F_0}{F} = 1 + K_{app}[Cu] \quad \text{where} \quad K_{app} = \left[\frac{F_0}{F} - 1 \right] [Cu]^{-1} \quad (6)$$

A plot of K_{app} versus $[Cu]$ yields a straight line with an intercept (I) of $K_D + K_S$ and a slope (S) of $K_S K_D$. Manipulation of these relationships, gives a quadratic equation

$$K_S^2 - K_S I + S = 0 \quad (7)$$

We analyzed the data for the complexes according to this equation (5) [24] (Fig. 9). In all cases, solutions to the quadratic equation are complex roots. Generally speaking, a completely unambiguous assignment of K_D and K_S requires fluorescence lifetime measurements [24]. Typically, for proteins the quenching constants are nearly identical [28].

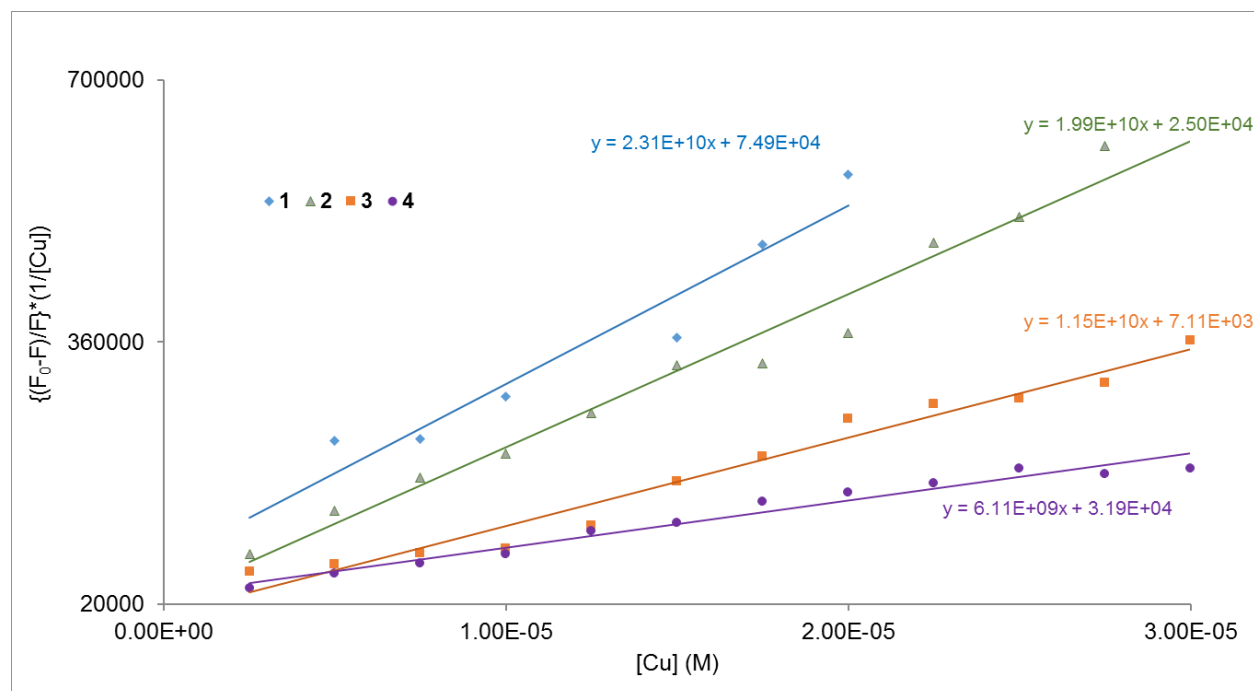


Fig. 9. Plot of the Stern-Volmer analysis according to equation (5)

As mentioned above, tryptophan amino acid residues have higher quantum yields than the two other fluorescent amino acids. Despite this, tyrosine, because it is typically present in larger numbers, may contribute significantly to the protein fluorescence. In the case of HSA with the eighteen tyrosine residues, one cannot completely eliminate tyrosine emission. Therefore, it is possible that there is more than one population of fluorophores accessible to the metal complexes and each residue can be differently accessible. In the situation where there is one population of fluorophores, one accessible and the other inaccessible to the quencher, deviation from linearity of the Stern-Volmer relationship is also observed [24]. Under these circumstances, the binding constant can be obtained from a modified Stern-Volmer (MSV) analysis [28].

$$\frac{F_0}{F-F_0} = \frac{1}{fK[Cu]} + \frac{1}{f} \quad (8)$$

This allows estimation of the apparent binding constant K for the process, from the ratio of the slope to intercept of a plot of $F_0/(F - F_0)$ vs. $1/[Cu]$. This plot is shown in Fig. 10. The calculated binding constants are $1.99 \times 10^5 \text{ M}^{-1}$, $2.02 \times 10^5 \text{ M}^{-1}$, $3.45 \times 10^5 \text{ M}^{-1}$ and $1.89 \times 10^5 \text{ M}^{-1}$ for **1**, **2**, **3**, and **4**, respectively. These values indicate that the complexes are strong binders to the protein.

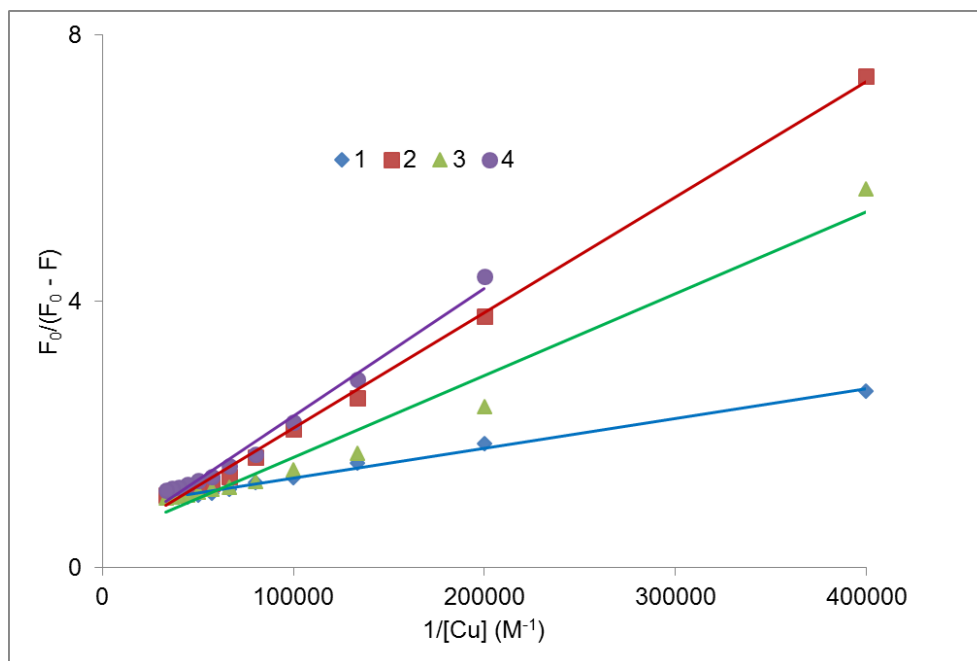


Fig. 10. Plot of the modified Stern-Volmer equation

Another possible reason for the upward curvature may be that with increasing binding as the concentration of the complexes increased, a change in the conformation of the protein results in the exposure of previously inaccessible fluorophores [30,31].

3.7 Anti-oxidant assays

Free radicals, particularly reactive oxygen species (ROS), can have a deleterious effect on cellular processes by, for instance, targeting biomolecules such as nucleic acids. The adverse effects will arise if the cell's natural anti-oxidant machinery is compromised so that it is incapable of neutralizing excess free radicals. There are a number of methodologies available for estimating the anti-oxidant capability of metal complex. One popular method is based upon the use of the stable free radical diphenylpicrylhydrazyl (dpph). This radical can be reduced via a reaction with a hydrogen atom donor. The reaction can be monitored by measuring the change in absorbance of the reaction mixture at 520 nm. This is the wavelength of maximum absorbance for the dpph molecule, that results from delocalization of the unpaired electron. The scavenging capacity was calculated from the following equation (9):

$$SC\% = \left[\frac{A_{\text{control}} - A_{\text{sample}}}{A_{\text{control}}} \right] \times 100\% \quad (9)$$

A_{control} is the absorbance of the control and A_{sample} is the absorbance of the sample. All the absorbances should be corrected for the blank. Fig. 11 show the variation of the scavenging capacity with the concentration of the complexes. Generally speaking, there is a saturation effect at the higher concentrations. The activities of the complexes are not spectacular; at the highest concentration studied, percent scavenging capacity is only 13-21%. Complex 2 showed the highest scavenging ability.

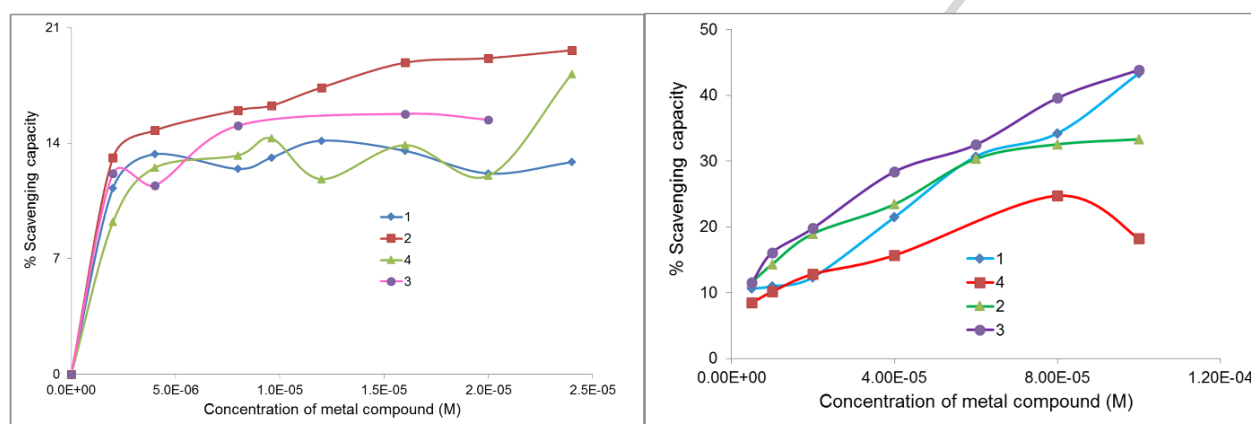


Fig. 11. Radical scavenging ability of the complexes by dpph assay (left) and nitric oxide assay (right)

Nitric oxide (NO) is another free radical that is an important chemical mediator with a variety of physiological functions. Like the ROS, NO exhibit these effects at low concentrations. At higher concentrations, it too can cause biological damage to tissues and organs. A number of disease conditions can then result. Because it is a potent vasodilator, sodium nitroprusside, $\text{Na}_2[\text{Fe}(\text{CN})_5\text{NO}]$, is a drug used to treat a variety of medical conditions including hypertension. The mode of action of this drug is the basis of the assay, which is the use of an aqueous solution that at physiological pH spontaneously generates nitric oxide. This nitric oxide interacts with oxygen to produce nitrite ions, the amount of which can be estimated using Griess' reagent. Consequently, the presence of any species that can scavenge the nitric oxide radical will result in reduced production of nitrite ions and a decrease in the absorption of such a mixture at 550 nm. The scavenging capacity was determined as above for dpph. The activity, from the standpoint of scavenging capacity, is higher against the nitric oxide radical relative to dpph. Complexes 1 and 3 show the highest activity of approximately 40% at the highest concentrations.

3.8 Antimicrobial assays

The antimicrobial activity of the compounds was studied with three protocols. The ligands were tested against five ESKAPE pathogens – *S. aureus* (MRSA), *E. coli*, *K. pneumoniae* (MDR), *A. baumannii*, and *P. aeruginosa*. These organisms are so called because they can ‘escape’ the common antibacterial regimens. Table 3 shows the results of the biological assays.

Table 3 Antimicrobial profile of the ligands and complexes

% inhibition		npTSC	MnpTSC	EnpTSC	PnpTSC
<i>Staphylococcus aureus</i> (MRSA)	Gram (+)	29.38	17.16	12.92	27.76
<i>Escherichia coli</i>	Gram (-)	-8.98	-12.93	-8.70	-5.23
<i>Klebsiella pneumoniae</i> (MDR)	Gram (-)	-0.72	-7.59	4.74	19.90
<i>Acinetobacter baumannii</i>	Gram (-)	4.44	-9.14	-4.09	7.86
<i>Pseudomonas aeruginosa</i>	Gram (-)	-19.37	2.27	1.44	1.57
<i>Candida albicans</i>	Yeast	9.81	2.75	3.58	1.03
<i>Cryptococcus neoformans</i>	Yeast	-13.48	-39.33	-37.11	-39.72
		1	2	3	4
<i>Pseudomonas aeruginosa</i>		21.9	92.2	6.25	
<i>Klebsiella pneumonia</i>		39.5	35.0	46.3	45.8
<i>Staphylococcus aureus</i>		15.8	2.86	34.2	17.8
<i>Escherichia coli</i>		34.7	54.7		75.4
<i>Enterococcus faecalis</i>			51.5	93.1	
<i>Bacillus cereus</i>		17.6 (131)		69.7 (117)	64.3 (118)

1, **2**, **3**, and **4** were tested at 22.9 μ M, 20.0 μ M, 20.0 μ M and 19.0 μ M respectively for *P. aeruginosa* and *K. pneumoniae*. For the other bacteria, the tested concentrations were 21.7 μ M, 20.0 μ M, 19.4 μ M and 19.6 μ M for **1**, **2**, **3**, and **4** respectively. For *B. cereus* the numbers in parentheses are the concentrations at which the complex was tested.

It is obvious that the ligands are not active (defined as > 80%) against these bacteria with the best compound being npTSC and PnpTSC against *S. aureus*. Negative inhibition values mean

that the growth rate is higher compared to the control (bacteria only, set to 0% inhibition). The complexes were tested against four of the same bacteria in addition to *B. cereus*. The first set of experiments involved determining the susceptibility of the bacteria to the complexes using the disc diffusion method and measuring the zones of inhibition. The only bacterial strain that displayed any growth inhibition was *S. aureus*. (Fig. 12). The inhibition zones were 16 mm, 10 mm, 11 mm and 10 mm for **1**, **2**, **3**, and **4**, respectively. This would classify the bacteria as resistant. In comparison, ampicillin, a clinically used antibiotic, exhibited a 39 mm zone of inhibition. The vehicle for the complexes, DMSO, did not inhibit growth of the bacteria.

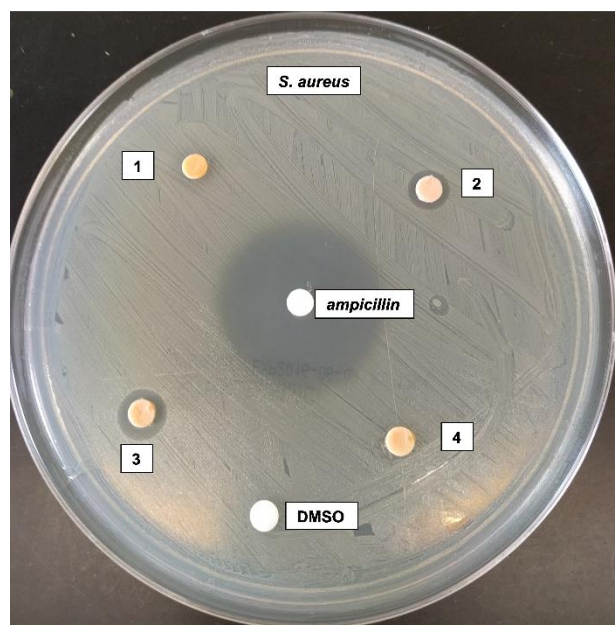


Fig. 12. Antibacterial activity of the complexes on the growth on *S. Aureus* as measured by the disc diffusion method.

To determine if the concentration on the discs was insufficient to cause inhibition, an experiment to determine the percent inhibition was done using a microdilution method. The results of this study are presented in Table B. It was observed that there is no pattern to the reactivity and an IC_{50} value could not be calculated. The values represent the inhibition at the lowest tested concentration. A possible reason for this is the absorption characteristics of the complexes. At the high or even medium concentrations, the absorption of the complexes at 600 nm (the wavelength of the analysis), is significant enough to affect that from the growing bacteria. This distorted the measurements leading to a lack of precision at these concentrations.

It is not exactly clear why the complexes or the ligands are not biological active. However, we can speculate on some possible reasons. Drug-likeness, the likelihood that a

compound will have useful therapeutic activity, is a qualitative concept used in drug design and is predicted from the molecular structure. The quantitative structure activity relationships (QSAR) attempt to correlate biological activity with the physiochemical properties of a drug. The properties are any structural, physical or chemical property of the drug. Probably the most common of these properties is lipophilicity, which is represented by the partition coefficient log P. Two other properties that are related to each other are molar refractivity (represented as CMR: $c =$ calculated) and the topological polar surface area (tPSA). The molar refractivity represents size and polarizability of a molecule. It is also related to the London dispersive forces that act in the drug-receptor interaction. The size of the molecule is also important. Most drugs enter cell membranes by passive transport and the rate of passive transport depends on the size of the molecules. The topological polar surface area (tPSA) is a convenient measure of the molecular polar surface area and is correlated with passive molecular transport through membranes and other drug transport properties. We have calculated, (using ChemDraw), the values for these three parameters for the thiosemicarbazone ligands. We assume that the complexes will have somewhat similar properties, likely bigger values since they include the metal ion. As is expected, the size of the ligands increases with alkyl substitution on the amine nitrogen. The CMR values are 6.945 cm³/mol, 7.407 cm³/mol, 7.873 cm³/mol and 9.456 cm³/mol for *npTSC*, *MnpTSC*, *EnpTSC* and *PnpTSC* respectively.

Generally speaking, drugs should be designed with the lowest possible log P. For oral bioavailability, this should be in the range -0.4 to +5.6. The calculated log P values for the ligands were 0.22, 0.65, 0.86 and 2.21 for *npTSC*, *MnpTSC*, *EnpTSC* and *PnpTSC* respectively. This pattern seems reasonable given the differences between the methyl, ethyl and phenyl groups with respect to polarity. Compounds with higher log P values are non-polar, with lower water solubility. The complexes should have higher log P values since there are two ligands and this might be the real reason for their poor antimicrobial activity – their poor aqueous solubility. This is likely true for the other properties as well.

The tPSA for the compounds show an interesting pattern. *npTSC* has a calculated tPSA of 120.68 Å² and the other three have the same value of 106.69 Å². It is interesting to note that the tPSA is actually smaller for the larger molecules. According to Veber's rule [32], these values should be from 40 to 130. The complexes are expected to be bigger than the individual ligands so the CMR and tPSA values are likely to be unfavorable. In fact, the calculated (from the DFT geometry optimization) volume for the complexes are 170.68 Å², 144.20 Å², 143.47 Å² and 141.25 Å² for **1**, **2**, **3** and **4** respectively. The values for the bigger complexes are at the top limit of drug-likeness. Veber's rules also suggest that molecules with hydrogen bonding

capability (acceptors and/or donors) greater than ten would have poor oral bioavailability. All the complexes possess sixteen hydrogen bond acceptors.

In addition to poor physiochemical characteristics, it is possible that the compounds do not significantly interact with common microbial biological targets. To investigate this possibility, we have computationally (molecular docking) studied the interaction of the complexes with two macromolecules that are targets for a variety of clinically used antibacterials.

3.9 Molecular docking interaction of complexes with biological targets

The thiosemicarbazone ligands used in this study, with their benzodioxole moiety, has a high degree of structural similarity to oxolinic acid, which is a member of the quinolone class of antibiotics. The quinolone antimicrobials targets DNA gyrase (topoisomerase II) and topoisomerase IV (Topo IV) [33-35]. These enzymes are related bacterial type II topoisomerases that have significant roles in DNA replication and cellular growth; they catalyze topological changes in the bacterial genome. The two enzymes have somewhat different roles [36] but are essential for bacterial growth. They also have susceptibilities to antibiotics that are species dependent [9]. Despite the poor antibacterial profile of the ligands and complexes, we thought it worthwhile to explore, through molecular docking models, to what extent the complexes can bind to these important enzymes. We expected that useful information could be obtained by looking at the binding constants along with the QSAR properties of the complexes. The molecular docking simulations were performed using the X-ray crystallographic structures of the DNA gyrase of *Staphylococcus aureus*, obtained from the Protein Data Bank (code 3G75) along with that of the parE subunit of topo IV obtained from the same source (code 3LNU). In the preparation of the topo II protein, the co-crystallized inhibitor was first removed from the structure before docking with the complexes. In both cases, the runs were carried out on a rigid (protein) molecule. The optimized geometric forms of the complexes were used in the docking simulations. The individual interactions were studied in order to obtain more detailed information. An examination of the information in Table 4 below reveals the general trend that the complexes bind stronger to the Topo IV than the DNA gyrase B. It is also interesting to note that compound **4** binds the strongest to the DNA gyrase B and Topo IV out of all four complexes, which is reflected by the most negative binding energy and the lowest dissociation constant. A look at the binding interactions between all four complexes and the macromolecule of interest provides further insight into the observed trends.

All of the complexes docked with DNA gyrase B, has the $-\text{NO}_2$ group on at least one of the TSC ligands playing an important role in the binding process. Figure A shows such

interactions for complex **4**. (The other complexes are shown in the ESI). The $-\text{NO}_2$ group is involved in conventional hydrogen bonding with a variety of amino acid groups present within the enzyme. For example, complex **1** exhibits a total of three conventional hydrogen bonding interactions: two between the $-\text{NO}_2$ on the first TSC ligand and the $-\text{NH}$ of TYR192 and one between the $-\text{NO}_2$ and the $-\text{NH}_2$ group of ARG217. Both sets of interactions are 1.63 Å. Complex **2** displays two conventional hydrogen bonding interactions between the $-\text{NO}_2$ on TSC1 and the protonated $-\text{NH}_2$ group of LYS170 (2.08 Å and 1.70 Å). **3** displays a single conventional hydrogen bonding

Table 4 Calculated binding energies and dissociation constants (kl) for the complexes with DNA gyrase B and Topoisomerase IV

Macromolecular Target → Compound ↓	DNA gyrase B		Topoisomerase IV	
	Binding Energy	kl	Binding Energy	kl
1	-7.05	6.79	-8.06	1.23
2	-6.68	12.61	-8.04	1.27
3	-6.29	24.65	-7.3	4.42
4	-7.25	4.82	-8.79	0.37

*Binding energies are reported in kJ/mol and dissociation constants are in micromolar units.

interaction between the $-\text{NO}_2$ of TSC1 and the $-\text{NH}$ of THR171 (1.78 Å). Lastly, for **4**, which is the complex demonstrating the strongest binding to DNA, there are a total of three conventional hydrogen bonding interactions. One of these interactions is between an oxygen on the $-\text{NO}_2$ of TSC2 and a hydrogen on the five membered ring of HIS143 (1.93 Å). The other two interactions are between the two oxygens on the $-\text{NO}_2$ group of TSC1 and two hydrogens on the protonated $-\text{NH}_2$ group of LYS170 (2.32 Å and 2.33 Å). It is observed that with increasing amount and strength of hydrogen bonding interactions between the $-\text{NO}_2$ group on the TSC ligand, the binding with DNA gyrase B becomes more favorable.

Other interactions between the complexes and DNA gyrase B are worth noting. In addition to conventional hydrogen bonding, the aromatic portion of the piperonal moiety present in the TSC ligand also show various interactions that can explain the binding energies. For

example, **1** exhibits two pi-interactions: one pi-anion between the aromatic ring of TSC2 and ASP225 (4.52 Å) and one pi-alkyl between the same location and ARG223 (4.68 Å). **2** has three pi-interactions, **3** has a single pi-interaction, and **4** has 4 pi-interactions, all of which are seen in Fig. 13 (or the ESI). Compound **4** exhibits the strongest binding to the DNA complex due to the amount and strengths of conventional hydrogen bonding interactions as well as the various pi-interactions that occur.

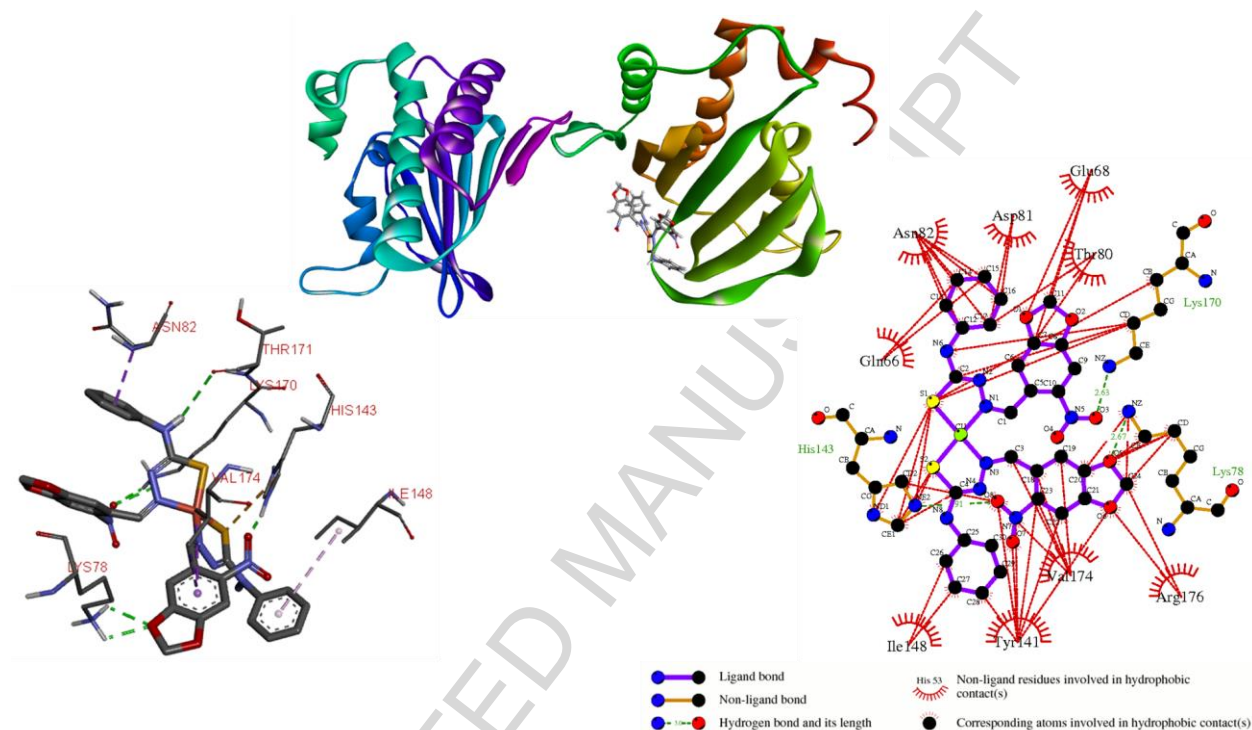


Fig. 13. Molecular interactions between complex **4** and DNA gyrase B

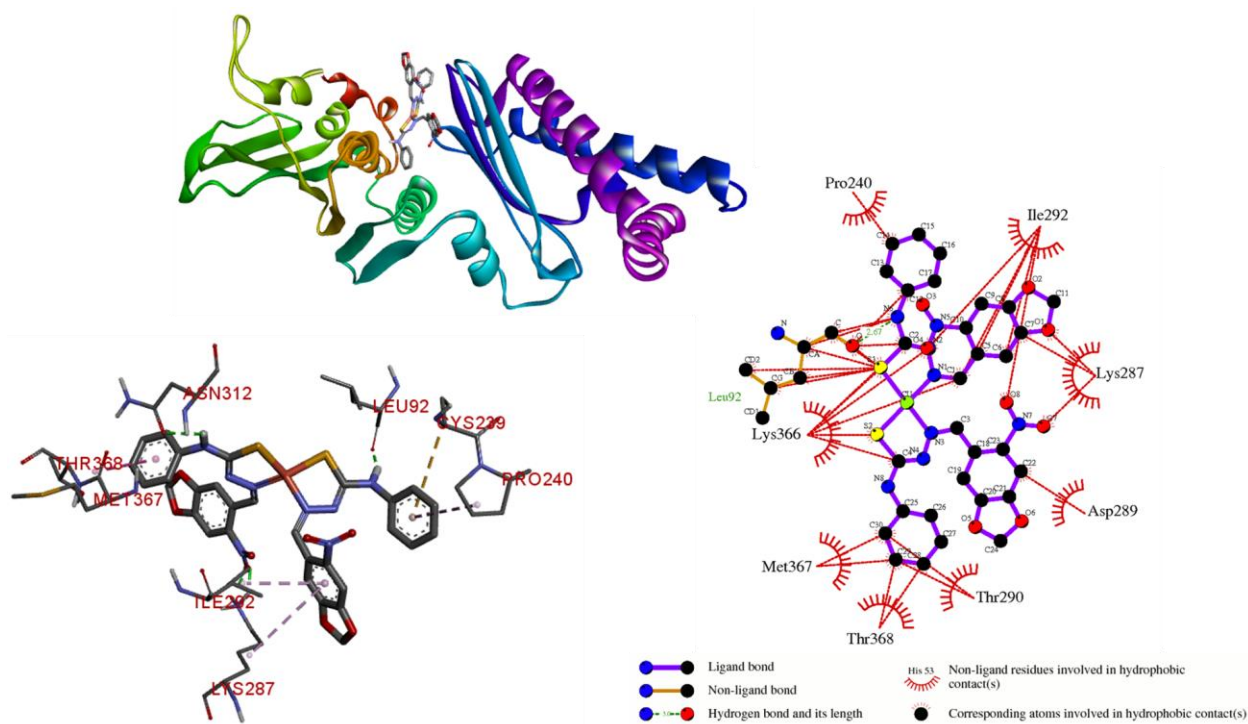


Fig. 14. Molecular interactions between complex **4** and Topoisomerase IV

As previously mentioned, the docked complexes appear to have a higher affinity for the topoisomerase IV enzyme compared to the DNA gyrase B enzyme. In a similar manner to the gyrase enzyme, the docked poses of topoisomerase IV with all of the complexes exhibit conventional hydrogen bonding interactions with at least one of the $-\text{NO}_2$ groups on the TSC ligand, which demonstrates the importance of this functional group in the binding process with these two enzymes (Fig. 14 for complex **4**). The complex with the most conventional hydrogen bonding interactions and other pi-interactions is **4**. There are four conventional hydrogen bonding interactions observed for this complex with this enzyme: one between the hydrogen on the $-\text{NH}$ of TSC1 and the oxygen on the carbonyl group of LEU92 (1.73 Å), one between the $-\text{NH}$ group on TSC2 and oxygen on the carbonyl group of ASN312 (3.01 Å), and two between two hydrogens on the protonated NH_2 group ($-\text{NH}_3$) of LYS287 and both oxygens on the $-\text{NO}_2$ group of TSC2 (1.86 Å and 1.91 Å). Additionally, there are five pi-interactions observed for **4** docked with topo IV: a pi-sulfur interaction between the sulfur on CYS239 and the aromatic ring on TSC1 (5.69 Å), a pi-alkyl interaction between the phenyl ring on TSC1 and the five membered ring on PRO240 (5.08 Å), two pi-alkyl interactions between the aromatic ring in the piperonal fragment and ILE292 (4.30 Å) and LYS287 (5.22 Å), and an amide pi-stacking interaction between phenyl ring of TSC2 and THR368 and MET367 (3.96 Å).

From the results of the docking studies, we conclude that all of the complexes exhibited an overall higher binding affinity for the topo IV versus the DNA gyrase B enzyme. Complex **4** has the most favorable binding of the four complexes with these two enzymes. One likely reason for the favorable binding observed in this complex, is the presence of the phenyl ring that is not present in the other complexes. This allows for more pi-interactions between the various groups that constitute the enzyme.

Conclusion

We have synthesized four novel thiosemicarbazones derived from 6-nitropiperonal. These ligands showed interesting coordination chemistry when ligated to a copper center. These complexes show that the ligands coordinate as the deprotonated thiol tautomer. The complexes bind to DNA and human serum albumin. The strength of the interaction suggested that the complexes were moderate binders to both DNA and HSA. No evidence was uncovered to unambiguously assign a mode of binding (such as intercalation) to DNA. Like the ligands, the complexes do not show outstanding antimicrobial profiles against the ESKAPE pathogens. This fact might be related to their pharmacokinetic characteristics; it is likely that they are unable to cross cell membranes. Calculated physicochemical properties, (such as the partition coefficient, molar refractivity and the topological polar surface area), of the ligands clearly show the enhanced influence of the substituent phenyl group relative to the smaller and electron donating alkyl groups. This point is also supported by the results of a computational study that indicated the complexes could bind to two intracellular macromolecules. These targets, topoisomerase IV and DNA gyrase, are important targets for clinically used antibiotics. It was observed that the complexes with the phenyl-substituted thiosemicarbazone binds strongest to the proteins. The results of the experimental and computational studies, might suggest that the complexes could serve as lead molecules whose properties could be optimized. The complexes also good antioxidant activity as elucidated from the dpph and the nitric oxide assays.

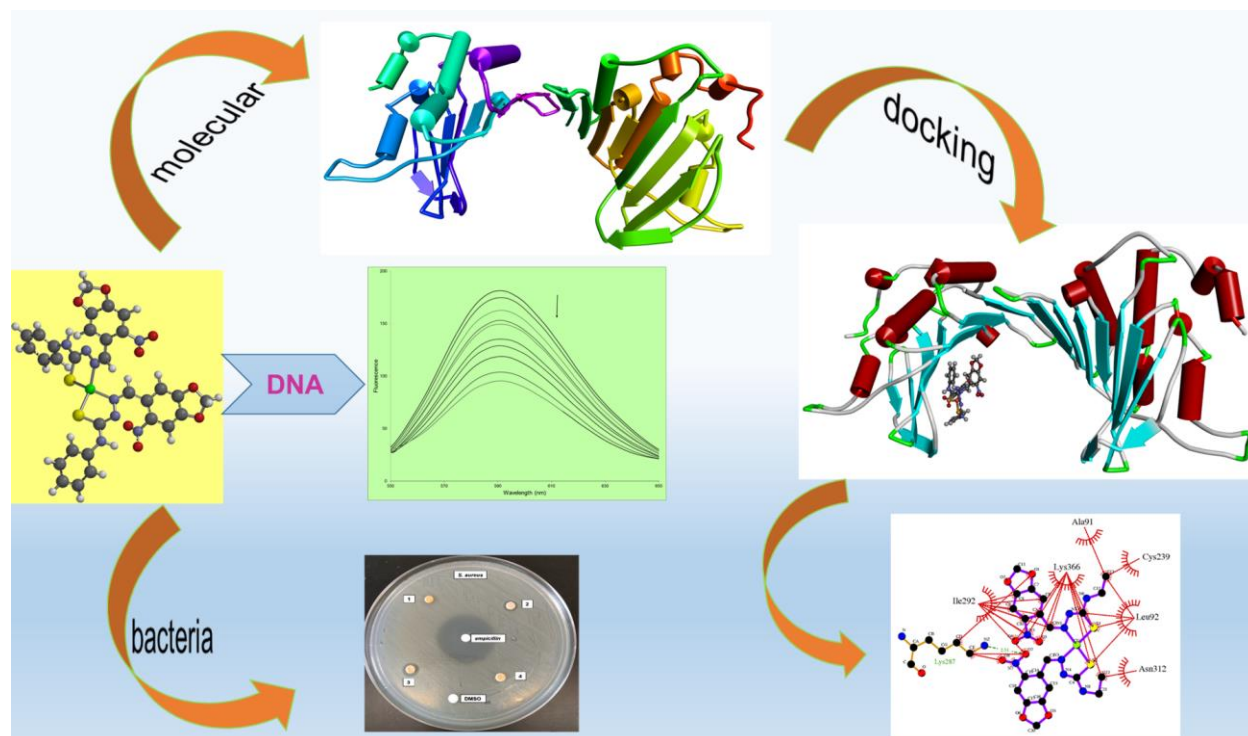
Acknowledgements

KRW would like to thank the Department of Natural Sciences at the University of Virginia's College at Wise for a Fellowship in the Natural Sciences to carry out this work. The authors would also like to thank CO-ADD (University of Queensland) for the antimicrobial assays and Bruker Biospin for the NMR analyses.

References

- [1] S. Dasari, P.B. Tchounwou, *Eur. J. Pharmacol.* **2014**, 740, 364 – 378.
- [2] D.X. West, I.H. Hall, K.G. Rajendran, A.E. Liberta, *Anti-Cancer Drugs*, **1993**, 4, 231 – 240.
- [3] O.E. Offiong, S. Martelli, *Farmaco* **1994**, 49, 513 - 518.
- [4] A.G. Quiroga, J.M. Perez, I. Lopez-Solera, J.R. Masaguer, A. Luque, P. Raman, A. Edwards, C. Alonso, C. Navarro-Ranninger, *J. Med. Chem.* **1998**, 41, 1399 - 1408.
- [5] D. Hadjipavlou-Litina, *Pharmazie* **1996**, 51, 468 - 470.
- [6] C.S. Allardyce, A. Dorcier, C. Scolaro, P.J. Dyson, *Appl. Organomet. Chem.* **2005**, 19, 1 - 10.
- [7] J. Qi, Y. Zhang, Y. Gou, Z. Zhang, Z. Zhou, X. Wu, F. Yang, H. Liang, *Molecular Pharmaceutics* **2016**, 13, 1501 - 1507.
- [8] V. Milacic, D. Chen, L. Giovagnini, A. Diez, D. Fregona, Q.P. Dou, *Toxicology and applied pharmacology* **2008**, 231, 24 – 33.
- [9] K. Drlica, X. Zhao, *Microbiology and Molecular Biology Reviews* **1997**, 61, 377 - 392.
- [10] F.A. Beckford, M. Shaloski, Jr., G. Leblanc, J. Thessing, L. C. Lewis-Alleyne, A.A. Holder, L. Li, N.P. Seeram, *Dalton Trans.* **2009**, 10757 - 10764.
- [11] F.A. Beckford, G. Leblanc, J. Thessing, M. Shaloski Jr., B.J. Frost, L. Li, N.P. Seeram, *Inorg. Chem. Commun.* **2009**, 12, 1094 - 1098.
- [12] M.E. Reichmann, S.A. Rice, C.A. Thomas, P.J. Doty, *J. Am. Chem. Soc.* **1954**, 76, 3047 - 3053.
- [13] R. Vijayalakshmi, M. Kanthimathi, V. Subramanian, B.U. Nair, *Biochim. Biophys. Acta*, **2000**, 1475, 157 - 162.
- [14] S. Krimm, J. Bandekar, *Adv. Protein Chem.* **1986**, 38, 181 - 364.
- [15] W.J. Geary, *Coord. Chem. Rev.* **1971**, 7, 81–122.
- [16] F.A. Beckford, A. Stott, A. Gonzalez-Sarrias, N.P. Seeram, *Appl. Organometal. Chem.* **2013**, 27, 425 – 434
- [17] Spartan'14, Wavefunction, Inc., Irvine, CA
- [18] S.J. Sabouncheia, P. Shahriarya, S. Salehzadeha, Y. Gholieea, D. Nematollahia, A. Chehreganib, A. Amanic, Z. Afsartalad, *Spectrochimica Acta. Part A, Molecular and Biomolecular Spectroscopy* **2015**, 135, 1019 - 1031.
- [19] A. Ambroise, B.G. Maiya, *Inorg. Chem.*, **2000**, 39, 4256-4263.
- [20] M. Jiang, Y.-T. Li, Z.-Y. Wub, Z.-Q. Liu, C.-W. Yan, *J. Inorg. Biochem.* **2009**, 103, 833 – 844.
- [21] Q. Liu, J. Zhang, M.-Q. Wang, D.-W. Zhang, Q.-S. Lua, Y. Huang, Y., H.-H. Lin, X.-Q. Yu, *Eur. J. Med. Chem.* **2010**, 45, 5302 - 5308.

- [22] W.J. Mei, J. Liu, C.K. Zheng, L.J. Lin, H.Chao, A.X. Li, F.C. Yun, L. N. Ji, *Dalton Trans.* **2003**, 1352 - 1359.
- [23] A.M. Pyle, J.P. Rehmman, R. Meshoyrer, C.V. Kumar, N.J. Turro, J.K. Barton, *J. Am. Chem. Soc.* **1989**, 111, 3051 - 3058.
- [24] J.R. Lacowicz, *Principles of Fluorescence Spectroscopy*, 3rd Ed. Springer, New York **2006**.
- [25] K.K. Ghosh, B.K. Sahoo, D. Jana, S. Dasgupta, *J. Inorg. Biochem.* 2008, **102**, 1711 - 1718.
- [26] J.P. Peberdy, J. Malina, S. Khalid, M.J. Haman, A. Rodger, *J. Inorg. Biochem.* **2007**, 101, 1937 – 1945.
- [27] M. Baldini, M. Belicchi-Ferrari, F. Bisceglie, G. Pelosi, S. Pinelli, P. Tarasconi, *Inorg. Chem.* **2003**, 42, 2049 – 2055.
- [28] R. Eftnik, C.A. Ghiron, *J. Phy. Chem.* **1976**, 80, 486 - 493.
- [29] R. Eftnik, C.A. Ghiron, *Anal. Biochem.* **1981**, 44, 199 - 227.
- [30] J. Weber, A.E. Senior, *Biochemistry* **2000**, 39, 5287 – 5294.
- [31] T.A. Wells, M. Nakazawa, K. Manabe, P.-S. Song, *Biochemistry* **1994**, 33, 708 – 712.
- [32] D.F. Veber, S.R. Johnson, H-Y. Cheng, B.R. Smith, K.W. Ward, K. D. Kopple, *J. Med. Chem.* **2002**, 45, 2615 – 2623.
- [33] B. Matjaz, P. Andrej, R. Miha, A. Gregor, T. Dusan, T. Solmajer, *J. Med. Chem.* **2012**, 55, 6413 – 6426.
- [34] C. Frédéric, S. Karkare, A. Maxwell, *Appl. Microbiol. Biotechnol.* **2011**, 92, 479–497.
- [35] J.A. Taylor, L.A. Mitchenall, M. Rejzek, R.A. Field, A. Maxwell, *PLoS ONE* **2013**, 8: e58010.



Graphical abstract

Highlights

- A series of four copper-thiosemicarbazone complexes were synthesized
- The complexes bind to DNA and human serum albumin
- The complexes display antioxidant capabilities
- Computational studies suggest the complexes can interact with biological molecules

ACCEPTED MANUSCRIPT